Magnetic Resonance in Medicine 50:830–838 (2003)

A PRESTO-SENSE Sequence With Alternating Partial-Fourier Encoding for Rapid Susceptibility-Weighted 3D MRI Time Series

Markus Klarhöfer,[1] Bixente Dilharreguy,[1] Peter van Gelderen,[2] and Chrit T.W. Moonen[1*]

A 3D sequence for dynamic susceptibility imaging is proposed which combines echo-shifting principles (such as PRESTO), sensitivity encoding (SENSE), and partial-Fourier acquisition. The method uses a moderate SENSE factor of 2 and takes advantage of an alternating partial *k*-space acquisition in the "slow" phase encode direction allowing an iterative reconstruction using high-resolution phase estimates. Offering an isotropic spatial resolution of 4 × 4 × 4 mm³, the novel sequence covers the whole brain including parts of the cerebellum in 0.5 sec. Its temporal signal stability is comparable to that of a full-Fourier, full-FOV EPI sequence having the same dynamic scan time but much less brain coverage. Initial functional MRI experiments showed consistent activation in the motor cortex with an average signal change slightly less than that of EPI. Magn Reson Med 50:830–838, 2003. © 2003 Wiley-Liss, Inc.

Key words: echo-shifting; sensitivity encoding; partial-Fourier; functional imaging

High temporal resolution in combination with large brain coverage is desirable in MR imaging studies like functional BOLD imaging or bolus tracking for perfusion investigations. Increasing the acquisition rate leads to an improved description of the hemodynamic response or the signal change caused by passing contrast media. At the same time it should allow for better correction for periodic physiological noise due to respiration and cardiac pulsation since the frequencies of the corresponding signal variations are better characterized.

Currently, multislice, single-shot EPI is widely used in experiments that require dynamic susceptibility-weighted imaging because of its robustness and availability. Despite the commonly accepted advantages of EPI, several disadvantages have been revealed. First, the long readout trains lead to susceptibility artifacts or geometric distortions, especially in lower brain regions. Second, the use of slice thicknesses of up to 10 mm leads to signal loss due to phase dispersion in the presence of susceptibility gradients. The recently proposed" z-shim" techniques (1–4) are able to recover these signal losses but decrease temporal resolution. Third, the multislice acquisition may result in inflow and slice-timing effects in functional studies. Recently, parallel imaging techniques like SENSE (5) and SMASH (6) have been used to accelerate MR imaging. However, note that with respect to imaging speed, a T_2^*-weighted EPI sequence with a given echo time has only limited benefit from these techniques since they would lead to dead times between excitation and data sampling.

The acquisition scheme of the PRESTO (7) sequence offers time-efficient 3D T_2^*-weighted imaging because of the echo-shifting principle. The method has already proven its feasibility in different functional (8–10) and perfusion studies (11,12). In combination with SENSE, whole brain coverage can be obtained in 1 sec (13) using a reduction factor of 2. Further scan time reduction by higher SENSE factors leads to highly increased spatially dependent noise related to the geometry of the coil array used (5). Therefore, we propose the combination of SENSE with a reduction factor of 2 and a novel partial-Fourier acquisition scheme to accelerate the PRESTO sequence.

The commonly used zerofilling approach to reconstruct partial-Fourier data introduces losses in spatial resolution. Iterative methods proposed, e.g., by Cuppen and van Est (14) and Liang et al. (15) that generate symmetric data in *k*-space by using phase estimates are able to restore these losses completely, if complete high-resolution phase information is present (15). In practice, low-resolution phase estimates are obtained by acquiring a few lines in addition to one-half of *k*-space. In the case of dynamic studies, full-Fourier data acquired prior to the time series can be used to correct the phases of the individual dynamic partial-Fourier scans (16). To take temporal changes of the high-resolution phase estimates into account, we propose to alternate the sampled half of *k*-space with each acquired volume. This allows a combination of two successive dynamic scans in order to calculate a high-resolution phase estimate that will be updated every second volume acquisition and allows for the correction of the individual partial-Fourier acquisitions. Since the 3D acquisition enables the separation of the fast phase encode ("blip") direction from the partial-Fourier direction, all echoes in the partial-Fourier direction are sampled at the same echo time. Therefore, no phase (T_2^*) evolution occurs in this direction, thus improving the quality of the phase estimates.

A combination of successive acquisitions of parts of *k*-space has previously been used in different applications. Scheidegger et al. (17) concatenated two half-echo acquisitions using different signs of the readout gradient to a pseudo-echo, thus allowing short echo times in flow imaging. Kellman et al. (18) proposed the use of alternating

[1]Imagerie Moléculaire et Fonctionelle: de la Physiologie à la Thérapie, ERT CNRS/Université Victor Segalen Bordeaux 2, Bordeaux, France.

[2]National Institute for Neurological Disorders and Stroke, NIH, Bethesda, Maryland.

Grant sponsor: European Union, Marie Curie Fellowship; Grant number: QLRI-CT-2000-52107 (to M.K.).

*Correspondence to: Chrit Moonen, Imagerie Moléculaire et Fonctionelle ERT CNRS/Université Bordeaux 2, 146 rue Léo-Saignat (Case 117), 33076 Bordeaux, France. E-mail: Chrit.Moonen@imf.u-bordeaux2.fr

Received 4 March 2003; revised 19 June 2003; accepted 23 June 2003.

DOI 10.1002/mrm.10599

Published online in Wiley InterScience (www.interscience.wiley.com).

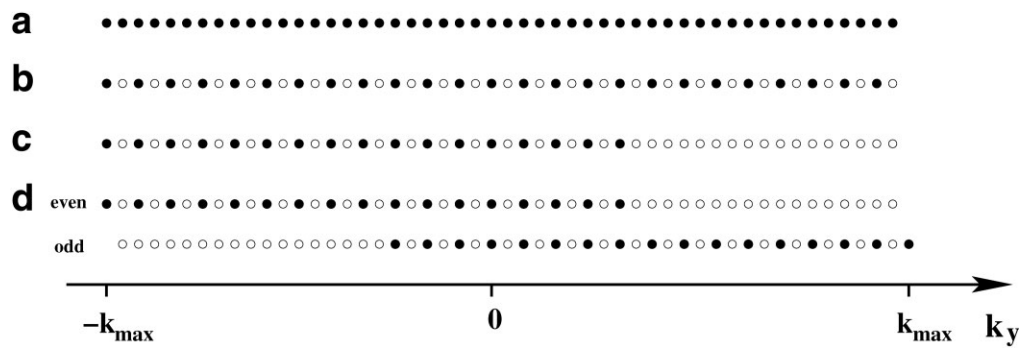

FIG. 1. Acquired *k*-space points (filled dots) in y-direction for full-FOV, full-Fourier (**a**); half-FOV (SENSE factor = 2), full-Fourier (**b**); half-FOV, partial-Fourier (**c**), and for half-FOV, partial-Fourier with alternating of the sampled *k*-space part (**d**). The number of acquired k_y-lines is reduced from 50 to 25 by the use of SENSE and in addition from 25 to 17 by partial-Fourier acquisition.

TRs to separately measure the odd and even *k*-space lines in a SENSE acquisition in order to obtain a low time resolution full-FOV reference.

In general, susceptibility-weighted dynamic MRI acquisition sequences can be judged by their amount of T_2^*-weighting and their temporal signal stability. Therefore, initial experiments with the proposed sequence focused on temporal signal behavior after various states of postprocessing, e.g., partial-Fourier reconstruction, use of navigator echoes, spatial registration, and correction for physiological motion. Furthermore, the novel PRESTO-SENSE sequence was compared qualitatively with an EPI sequence in a functional motor experiment.

MATERIALS AND METHODS

MR Acquisition

Experiments were performed on a Philips Intera 1.5 T system using a 6-channel headcoil. The maximum gradient strength, G_{max}, was 23 mTm^{-1} and the slew rate, S_{max}, was 120 $Tm^{-1}s^{-1}$.

Imaging parameters of the PRESTO sequence were: FOV = 25.6 × 20.0 × 12.0 cm^3, matrix = 64 × 50 × 29, TR = 29 ms, TE_{eff} = 44 ms, flip angle = 11°, scan time per volume = 0.5 sec. To avoid chemical shift artifacts, a water-selective excitation was applied using a binomial (1-2-1)-RF pulse. The acquisition bandwidth in read direction was 145 kHz and the length of the readout train 19 ms. Ramp-sampling was performed during half of the time needed to alternate the readout gradient. A navigator echo was acquired prior to each echo train in order to improve temporal signal stability (19,20). The use of SENSE and partial-Fourier acquisition reduced the number of acquired *k*-space lines in the y-direction (left–right) from 50 to 17 (see Fig. 1). The sequence was programmed in a way to acquire with each dynamic scan alternately the left and the right 70% of *k*-space in y-direction. The fast phase encoding ("blip"-direction) was performed along the z-direction (head–foot).

For comparison, a standard no-SENSE full-Fourier multislice EPI sequence with the following parameters was used: FOV = 25.6 × 20.0 cm^2, matrix = 64 × 50, TR = 500 ms, TE_{eff} = 44 ms, flip angle = 56°. Keeping the scan time per volume at 500 ms, five slices with a thickness of 4 mm could be acquired. Fat suppression was performed with a frequency selective inversion recovery method. The readout train of the EPI sequence had a length of 37 ms, the acquisition bandwidth was 110 kHz.

To investigate the temporal signal behavior of sequences with higher SENSE factors, a full-Fourier PRESTO protocol with a reduction factor of 3 in left–right direction was used. A 2D SENSE protocol with lower SENSE factors in two directions (21) was not feasible with the given coil geometry because it would require performing the readout in the z-direction. The resulting protocol would not be optimal with respect to imaging speed since the z-direction (head–foot) exhibits the smallest extension of the human brain.

During imaging, respiration and cardiac rate were recorded with a respiration sensor and a pulse oximeter for later use in a physiological noise correction algorithm.

Image Processing

To obtain the PRESTO images, two successive dynamic scans were reconstructed with the iterative Cuppen method using high-resolution phase estimates obtained by combining their complementary *k*-space parts (see Fig. 2). *k*-Space lines, acquired with both even and odd dynamic volume acquisitions, were averaged in the combination process.

In the Cuppen algorithm, the original data is inverse Fourier-transformed to the image domain, then conjugated and multiplied by $\exp(i2\Phi_{x,z}(y))$, where $\Phi_{x,z}(y)$ represents the phase estimate obtained by inverse Fourier transformation of the high-resolution reference data. A Fourier transformation back to the frequency domain results in data which are used to fill the missing *k*-space part of the original data. This process was repeated four times, whereby during the last iteration the merging of the calculated and original data included a linear weighting scheme applied to five *k*-space lines in order to avoid Gibbs ringing (15).

Depending on the magnetic field homogeneity, intensity differences occurred between even and odd images due to different *k*-space coverage (see Fig. 3). An intensity correction was applied by dividing all voxel values of odd images pic_odd_{2i-1} (x,y,z) by the ratio of the average voxel

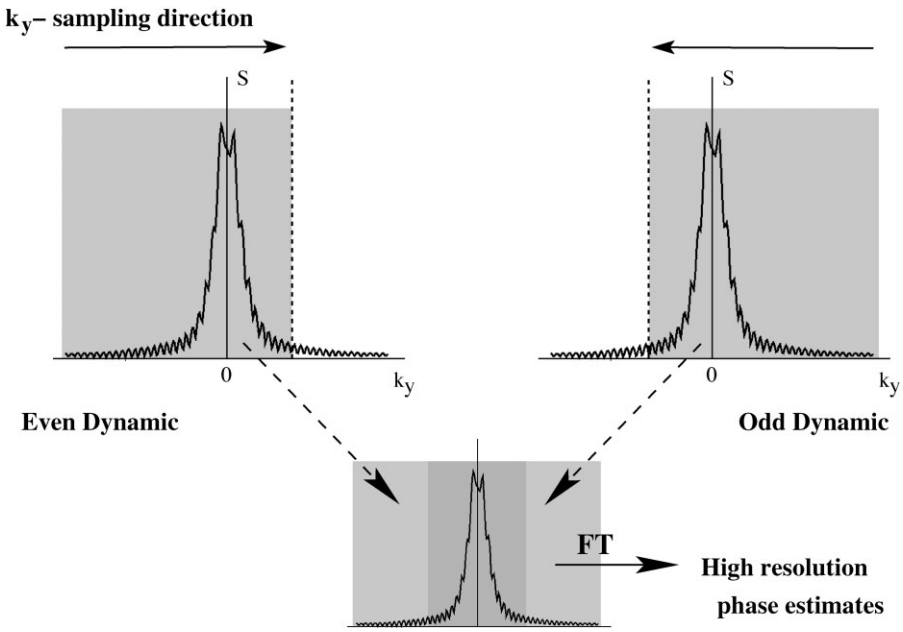

FIG. 2. Construction of reference data which are inverse Fourier-transformed to obtain high-resolution phase estimates for the Cuppen partial-Fourier reconstruction. Sampled *k*-space for even and odd dynamic scans is shaded. The data of two successive dynamic scans that cover alternately both parts of *k*-space are combined, whereby lines acquired with both acquisitions are averaged (dark shade).

values for odd and even images ($2/n \cdot \sum_{i=1}^{n/2} pic\_odd_{2i-1}$(x, y, z) and $2/n \cdot \sum_{i=1}^{n/2} pic\_even_{2i}$ (x, y, z), respectively):

$$pic\_odd_{corr,2i-1}(\mathrm{x},\mathrm{y},\mathrm{z}) = \frac{pic\_odd_{2i-1}(\mathrm{x},\mathrm{y},\mathrm{z})}{\frac{\sum_{i=1}^{n/2} pic\_odd_{2i-1}(\mathrm{x},\mathrm{y},\mathrm{z})}{\sum_{i=1}^{n/2} pic\_even_{2i}(\mathrm{x},\mathrm{y},\mathrm{z})}},$$
$$i = 1, \ldots, n/2 . \quad [1]$$

Here n denotes the total number of acquired dynamic scans (odd and even).

Two slices at both edges of the 3D slab were discarded because of folding artifacts due to nonrectangular excitation profiles. Images were reconstructed with and without the use of navigator echoes in order to investigate their influence on signal stability. The next postprocessing step consisted of registering the image time series to the last dynamic scan. For this, a pyramidal approach proposed by Thevenaz et al. (22) was used. In a last step, the recorded physiological information was used in the RETROICOR (23) algorithm in order to decrease periodic signal changes due to respiration and heartbeat.

After each of the aforementioned postprocessing steps, the temporal signal stability averaged over the whole brain was calculated. First, all voxels on the brain surface were discarded, since they often show high signal fluctuations due to slight subject motion. The (temporal) standard deviation of all remaining voxels (~16,000 in total) was then normalized to the mean voxel value (24). The small signal changes in activated regions had no significant influence on the signal stability averaged over the acquired brain volume. Therefore, all presented stability results were obtained from the functional MR data.

Navigator echoes were also used for the EPI sequence. The dynamic scans were corrected for motion and physiological noise in the same manner as the PRESTO images. Temporal stability averaged over the five acquired slices was calculated after all postprocessing steps.

fMRI Experiments

The functional experiment consisted of a block motor paradigm with four rest and three activation periods. Each period had a duration of 20 sec corresponding to 40 dynamic scans. Numbers from 2 to 5 were presented

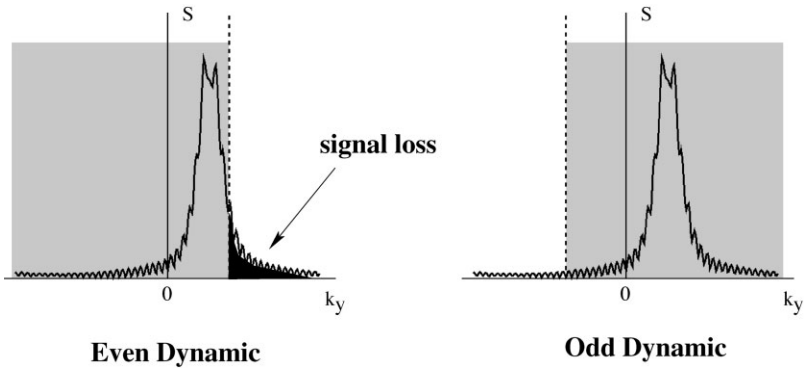

FIG. 3. Signal loss in the case of magnetic field inhomogeneities in y-direction due to susceptibility gradients. If, e.g., for an even dynamic scan, the resulting center of *k*-space for a given voxel is shifted in the direction of the unsampled part of *k*-space, signal loss will occur for all even dynamic scans. However, the alternating sampling scheme recovers this signal loss for all odd dynamic scans. An intensity correction has to be applied to use both even and odd acquisitions in dynamic imaging.

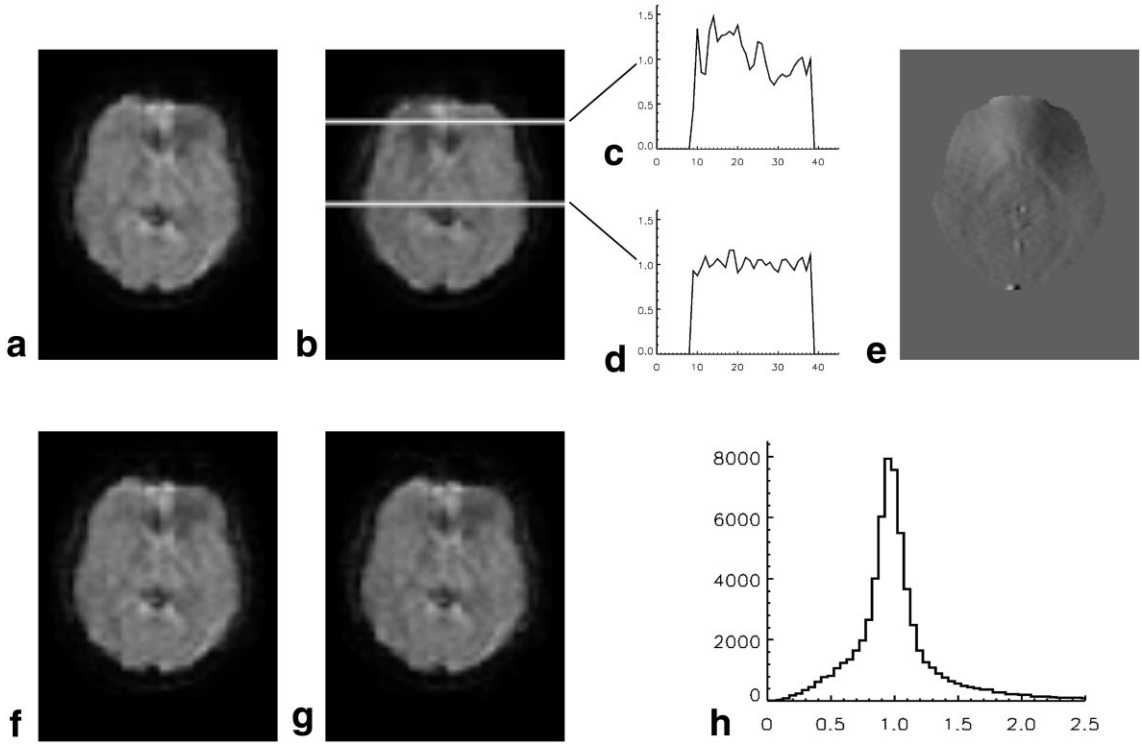

FIG. 4. Effect of susceptibility gradients on image intensity of alternating dynamic scans. **a:** One slice above the frontal lobes out of the volume obtained by averaging all even dynamic scans. **b:** As **a** for the average odd volume. **c,d:** Two magnitude profiles of a row of the intensity correction matrix calculated from the average even and the average odd dynamic acquisition. The magnetic field gradient in left–right (y-) direction of the present slice is shown in **e**. One even and one corrected odd dynamic scan are displayed in **f** and **g**, respectively. The histogram in **h** shows the distribution of the magnitude values of the correction matrix for the full 3D volume.

randomly to the subjects via a screen in the magnet room during the activation periods. The subjects had to tap the corresponding finger of the right hand against the thumb. The total duration of the experiment was 2 min 20 sec. It was performed once using the proposed PRESTO sequence and once using EPI. The order of the used sequences was alternated for different subjects. Five subjects participated in the study.

A correlation analysis (25) was performed to identify activated voxels. A correlation threshold of 0.26 was chosen, corresponding to a *P*-value of 1×10^{-5}. The image time series were not filtered temporally and neither clustering nor correction for multiple comparisons was applied to the functional maps.

RESULTS

Figure 4 illustrates the signal behavior in the partial-Fourier direction in the presence of strong susceptibility gradients. In Fig. 4a,b, one slice of the average even and the average odd 3D volume is shown. For even dynamic scans (k_y-direction from $-k_{y,max}$ to $0.4 \times k_{y,max}$) a signal loss occurs in a right frontal region of the brain, whereas for odd dynamic scans (k_y-direction from $+k_{y,max}$ to $-0.4 \times k_{y,max}$) the image intensity is diminished in a left frontal region. This alternate signal loss is caused by susceptibility gradients which shift the *k*-space center out of the acquisition window. To clarify this effect, Fig. 4e shows the magnetic field gradient in left–right (y-) direction in

Table 1
Temporal Signal Stability of the Partial-Fourier PRESTO-SENSE Sequence After Different Steps of Postprocessing

Subject	Raw	Even	Odd	Corr	Navi	Realign	Physcorr
1	5.55	2.53	2.63	2.65	2.17	2.16	2.08
2	5.54	2.32	2.34	2.37	2.35	2.34	2.27
3	5.12	2.46	2.54	2.53	2.30	2.25	2.18
4	5.39	2.73	2.69	2.76	2.32	2.29	2.21
5	5.20	2.34	2.25	2.34	1.98	1.94	1.87
Average	5.36 ± 0.20	2.48 ± 0.17	2.49 ± 0.19	2.53 ± 0.18	2.22 ± 0.15	2.20 ± 0.16	2.12 ± 0.16

For the five subjects the values are averaged over the whole brain (except edge voxels). Signal stability is given before intensity correction for alternate sampling of *k*-space (raw) and for all even and all odd dynamic scans (even, odd). The next columns show the results for the intensity-corrected time series (corr), the inclusion of navigator echoes (navi), the application of a motion correction algorithm (realign), as well as the temporal signal stability after physiological correction using RETROICOR (physcorr).

Table 2
Comparison of the Temporal Signal Stability of the Proposed PRESTO Sequence With That of a Standard EPI Technique

Subject	PRESTO 25sl			EPI 5sl	EPI 5sl
	Whole brain	Motor brain	Visual area	Motor area	Visual area
1	2.08	1.69	2.24	1.84	2.20
2	2.27	2.08	2.44	1.89	2.13
3	2.18	2.00	2.30	2.21	2.65
4	2.21	2.02	2.52	2.34	2.26
5	1.87	1.67	2.05	1.70	2.40
Average	2.12 ± 0.16	1.89 ± 0.20	2.31 ± 0.18	2.00 ± 0.27	2.33 ± 0.21

In the EPI case due to reduced spatial coverage, two time series were performed to obtain results for motor and visual areas, whereas for PRESTO the corresponding regions where cut out of the 3D volume of one experiment.

the same slice. Figure 4c,d shows two magnitude profiles in the left–right direction of the correction matrix for the considered slice. It can be seen that only minor magnitude corrections were performed in regions with low field gradients in the y-direction, whereas significant corrections were applied in the frontal part of the slice. In Fig. 4f,g, one even and one intensity-corrected odd dynamic scan are displayed. Figure 4h shows the distribution of the magnitude of the applied correction factors for the whole 3D volume.

The temporal stability, *TS*, averaged over the whole brain is given in Table 1 following the different steps of postprocessing. The applied intensity correction to compensate for different *k*-space coverage during the alternate sampling improved *TS*, averaged over five subjects, by more than 50%. The navigator echoes lead to a further important improvement of the stability of ~12%. Motion correction resulted only in minor refinements of *TS* (~1%), whereas the finally applied physiological correction lead to a further average stability enhancement of 3.6%. The finally obtained temporal stability averaged over all subjects was 2.12 ± 0.16%, whereby 16,064 ± 911 voxels of each subject were considered.

Table 2 shows a comparison of the temporal stability of the PRESTO sequence averaged over the whole brain and over five slices, including motor or visual cortices, with that obtained with EPI in five transversal slices covering the motor or visual cortex. In the EPI case the slice stacks were positioned parallel to the 3D slab of the PRESTO sequence. With EPI a mean stability of 2.00 ± 0.27 in upper brain regions and of 2.33 ± 0.21 in lower regions was obtained. For both EPI and PRESTO, *TS* was ~15% lower in slices at the position of the visual cortex than in those containing motor areas.

The full-Fourier PRESTO sequence using a SENSE factor of 3 resulted in an average signal stability of 3.58%. Figure 5a shows a histogram visualization of the signal stability in the brain for both sequences. For the higher SENSE factor, the maximum of the distribution is shifted from ~1.6% to 2.6% and the distribution exhibits a broad shoulder with increased normalized standard deviations corresponding to multiple folded areas in the brain. Figure 5b shows the spatial dependence of the stability for the partial-Fourier and the full-Fourier PRESTO sequence with increased acceleration factor. In both cases the stability map reflects the geometry factors of the SENSE reconstruction. The profiles of the stability maps shown in Fig. 5c demonstrate

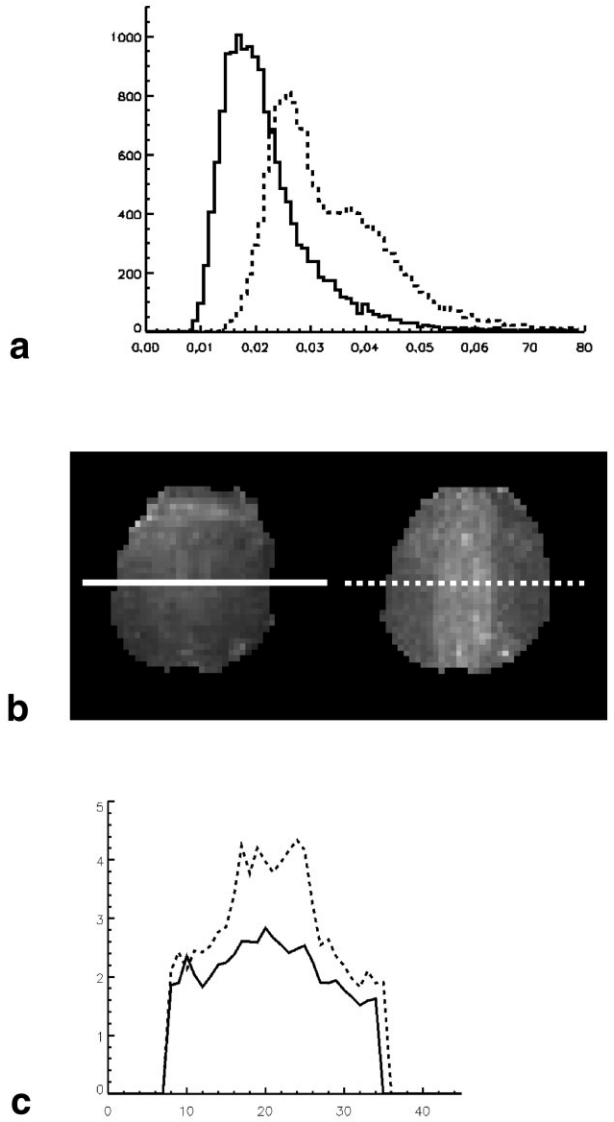

FIG. 5. Temporal signal stability of the proposed sequence (solid line) compared to that of a PRESTO sequence using a SENSE factor of 3 (dashed line). The histograms in **a** show the distribution of calculated stability values for both sequences (SENSE factor 2, partial-Fourier: solid line; SENSE factor 3, full-Fourier: dashed line). In **b**, temporal signal stability is converted to gray-scale values for a given slice of the proposed PRESTO (left) and the PRESTO-SENSE = 3 sequence (right). The spatial distribution of the signal stability clearly reflects the geometry factors of the SENSE reconstruction. **c:** The marked profiles in **b** for better visualization.

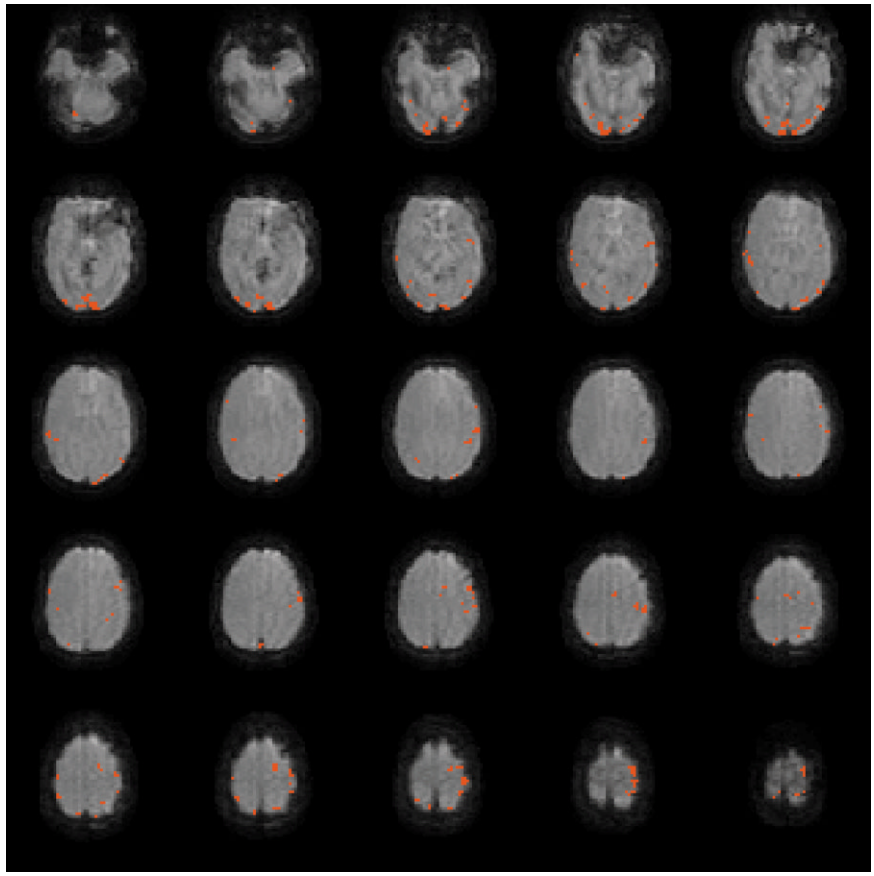

FIG. 6. Twenty-five central slices out of the 3D volume acquired in 0.5 sec with the partial-Fourier PRESTO-SENSE sequence (Subject 5). Activated voxels are overlaid in red and are predominantly located in primary and supplementary motor areas and the visual cortex.

the decrease of temporal stability, especially in the center of the images, where 3-fold folding occurred.

The proposed sequence results in isotropic $4 \times 4 \times 4$ mm^3 voxels and covers the whole brain including parts of the cerebellum. Twenty-five transversal slices of the first dynamic scan of a functional experiment (Subject 5) are displayed in Fig. 6. The voxels classified as activated according to the correlation analysis are overlaid in red. For all volunteers, activated voxels were found in motor and visual cortices. In three subjects SMA activation was found.

Figure 7 shows the activated voxels obtained with PRESTO and EPI in the motor area for Subject 2. Voxels are also marked in orange for PRESTO that survive a correlation threshold of 0.19 corresponding to a *P*-value of 1×10^{-3}. Except for one subject, EPI resulted in a higher number of activated voxels and in a larger signal change of these voxels during activation.

Figure 8 shows the signal time-course obtained with PRESTO averaged over all activated voxels for Subject 5. Averaged over all subjects, a mean signal change of 1.53% in five slices in the region of the motor cortex was observed with PRESTO and of 2.19% with EPI. Table 3 summarizes numerical results such as number of activated voxels and percentage signal change of the functional experiments.

DISCUSSION

To achieve rapid susceptibility-weighted imaging of the whole brain, we propose using PRESTO in combination

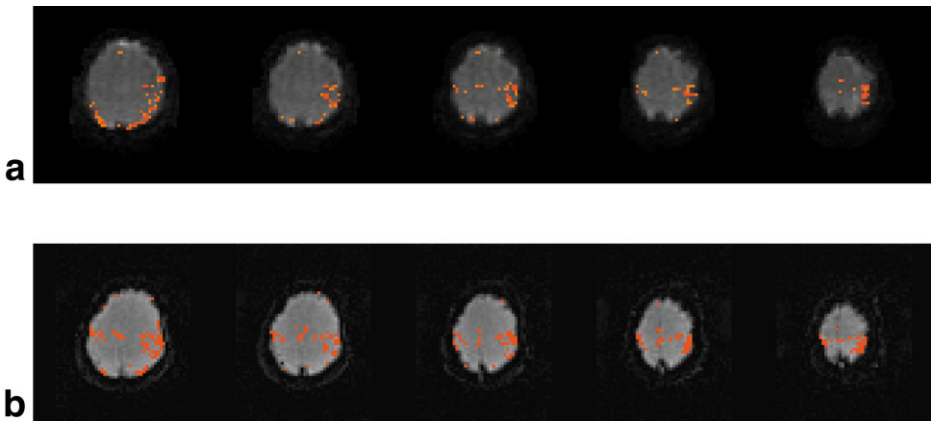

FIG. 7. Activated voxels for the partial-Fourier PRESTO-SENSE sequence (**a**) and a full-Fourier no-SENSE EPI protocol (Subject 2). Voxels marked red survived a correlation threshold of 0.26, the threshold for orange voxels in **a** was 0.19. Note that for **a** only five slices out of a total of 25 were selected corresponding to the location of the EPI slices in **b**.

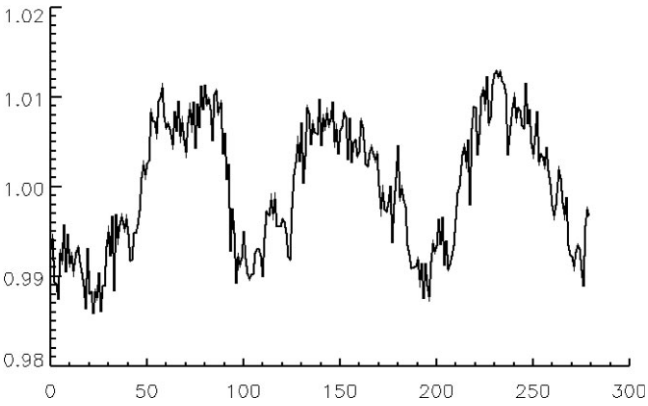

FIG. 8. Signal time-course averaged over all 402 activated voxels of Subject 5. Mean signal change due to activation was 1.3%.

with parallel imaging (SENSE) and partial-Fourier acquisition.

While echo planar-type sequences can take advantage of parallel imaging techniques with respect to image quality (fewer distortions due to shorter readout trains), or achievable spatial resolution per imaging time, or acoustic noise (use of smaller readout bandwidth and lower gradients/switching rates while keeping imaging time constant) (26), the necessity of long echo times limits the possibilities to shorten total imaging time in susceptibility-weighted imaging with EPI. This is due to the fact that the effective echo time of standard EPI sequences occurs after one-half of the total readout train. If parallel imaging methods are used to shorten the acquisition window, the readout train will be shortened symmetrically around the echo time. For a fixed TE, this introduces dead times between excitation and data acquisition. However, the echo-shifting principle of PRESTO fills the waiting periods with further sequence parts and therefore enables time-efficient use of parallel imaging techniques in T_2^*-weighted applications. In addition, as a multishot method, PRESTO generally uses shorter readout trains, which makes it less sensitive to macroscopic susceptibility artifacts than single-shot EPI techniques.

An important criterion for the quality of dynamic time series is signal stability over time. In our experiments, an acceleration factor of 2 lead to a slight additional signal loss of a few percent only, whereas a SENSE factor of 3 resulted in up to 60% signal loss in regions where the image was folded three times. This reduced SNR results in lower and spatially dependent temporal stability, which may hinder statistical evaluation. Therefore, a moderate acceleration factor of 2 was chosen for this study.

Despite being a multishot technique and despite the high sensitivity to motion caused by the crusher gradients that shift the echo signals, our experiments show that the temporal stability of the implemented PRESTO method was comparable to that of a single-shot EPI sequence. The use of navigator echoes, the low number of excitations, and the short total acquisition duration per dynamic scan (the latter two for a 3D volume) may contribute to this finding. In addition, the crusher gradients that shift the echo signal of the PRESTO sequence may diminish signal fluctuations caused by fast-moving blood and therefore may help to improve temporal stability.

The comparisons between partial-Fourier PRESTO-SENSE and EPI in this article are meant to demonstrate the properties of the new technique by comparing them with those of a well-known acquisition method. Therefore, a full-FOV, full-Fourier EPI sequence was chosen instead of a SENSE-EPI protocol which might have rendered the considered sequences more similar but would penalize the EPI protocol with respect to SNR. Note that precise quantitative comparisons between the proposed multishot 3D and a single-shot 2D technique are nearly impossible. Due to different TR and flip angles, signal contributions, e.g., by CSF, are different. Furthermore, slice definition differs from 2D to 3D imaging, as well as inflow effects. In addition, the presence and orientation of geometric distortions differ between the considered sequences.

High-quality partial-Fourier images were obtained by the iterative Cuppen reconstruction using high-resolution phase estimates. The alternating acquisition scheme allowed an update of the phase estimates every two dynamic scans. Phase variations during the time series are therefore taken into account. Note that the time resolution of the partial-Fourier acquisition is maintained, since the phase maps were only used in the symmetrization process of the partial-Fourier data. The frequency of updating phase maps (1 Hz) is half that of the volume acquisition frequency (2 Hz).

In fast 2D methods that acquire echo trains, T_2^*-evolution and off-resonance effects hinder the determination of phase estimates for the use in the Cuppen reconstruction algorithm. The 3D acquisition of the proposed PRESTO technique allowed the separation of the fast phase encode

Table 3
Number of Activated Voxels and Activation-Related Signal Change for Partial-Fourier PRESTO-SENSE and EPI

Subject	Number of activated voxels			Average signal change		
	PRESTO		EPI	PRESTO		EPI
	25sl	5sl	5sl	25sl	5sl	5sl
1	250	70	92	1.65	1.22	1.43
2	204	79	252	1.34	1.31	2.45
3	988	272	175	1.97	1.86	2.12
4	1240	300	891	1.97	1.96	3.21
5	402	88	254	1.29	1.30	1.76
Average	617 ± 468	161 ± 114	333 ± 319	1.64 ± 0.33	1.53 ± 0.35	2.19 ± 0.68

For PRESTO results are given for the region corresponding to the area covered by the EPI sequence, as well as for the full 3D volume.

from the partial-Fourier direction. Therefore, no TE evolution is present in the partial-Fourier direction, allowing good phase estimates for the calculation of the unsampled *k*-space part.

Magnetic field gradients due to susceptibility changes, e.g., in the vicinity of the frontal lobes, may result in signal loss and/or geometric distortions if T_2^*-weighted sequences are employed. Several methods have been proposed to reduce susceptibility-related signal loss. These include the use of higher spatial resolution to reduce the B_0 changes across voxels (27,28) and in the case of anisotropic 2D imaging (slice thickness > in-plane resolution), the application of tailored RF-pulses (29) or z-shimming techniques (1–4). Disadvantages of these methods are longer imaging times (increase of spatial resolution, z-shimming) or diminished SNR (tailored excitation). The z-shim problem reveals another advantage of 3D acquisition techniques. Since they generally use smaller section thicknesses than 2D acquisitions, more signal will be retained in object regions affected by susceptibility gradients (4).

For the proposed isotropic 3D PRESTO sequence, the direction of partial-Fourier encoding is most prone to susceptibility-related signal loss if the magnetic field gradient shifts the maximum of *k*-space in the direction of the incompletely sampled *k*-space half (cf. Fig. 3). However, as long as the shifted signal rests in the window that would be acquired with a full-Fourier acquisition, the next dynamic scan will record it because of the alternating sampling scheme. Clearly, this will lower the achieved "effective" temporal resolution for the affected region, but it may be an advantage over classical partial-Fourier acquisition schemes, where the considered signal would be lost for all dynamic scans. Whereas a moderate shift of the signal maximum in *k*-space influences the image phase, it has only minor effects on spatial resolution and signal strength (30,31). The applied intensity correction of the odd dynamic scans takes into account the different *k*-space coverage of even and odd volume acquisitions for moderate shifts of the signal maximum in the k_y direction of *k*-space. However, it cannot correct for signal loss or artifacts caused by severe susceptibility gradients that shift the signal in *k*-space out of the region covered by even or odd dynamic scans.

There are further advantages of the employed 3D acquisition scheme. First, it is less prone to inflow effects than multislice techniques (8). Second, in a 3D acquisition most of the signal (the central part of *k*-space) is acquired in a short time window. Therefore, no slice timing correction by interpolation techniques is necessary in the case of studies that require exact timing information like event-related fMRI or bolus tracking. Third, a 3D acquisition results in an image volume that is not corrupted by non-rectangular slice profiles or out-of-plane motion.

The obtained high temporal resolution of 0.5 sec should allow a good characterization of dynamic signal changes caused, e.g., by the hemodynamic response in fMRI or a passing bolus of contrast agent in perfusion studies. Furthermore, an acquisition rate of 2 Hz enables an accurate sampling of signal changes with frequencies up to 1 Hz, e.g., in the range of the cardiac frequency of our healthy volunteers. Therefore, the achieved temporal resolution allows good correction for physiological noise using, e.g., RETROICOR.

Despite a further reduction of scan time, the use of higher degrees of undersampling resulted in an unacceptable decrease in signal stability in our experiments. Nevertheless, higher acceleration factors may be feasible when head coils with even more elements become available. In this case, the proposed partial-Fourier acquisition scheme will still result in a scan time reduction, since it is independent of the parallel imaging approach.

In the functional feasibility studies, a fixed correlation threshold was used for all volunteers and both acquisition techniques. The studies showed significant variations in the number of activated voxels and the average percentage signal change between the subjects that did not depend on the sequence used. This is in line with the well-known intersubject variability of fMRI. In addition, the results of the functional study show that the number of activated voxels as well as the average percentage signal change obtained with PRESTO are consistently lower than those obtained with EPI. It has been suggested (32) that signals of large veins (diameter of about 1 mm) are suppressed due to the additional gradient pulses used for echo shifting. This inherent suppression may be an advantage if the downstream BOLD effect in large veins is to be suppressed.

CONCLUSION

In this article an alternating partial-Fourier sampling scheme was presented that enables the use of high-resolution phase estimates in iterative reconstruction algorithms. A fast susceptibility-weighted 3D technique was obtained by combining this method with the PRESTO sequence and parallel imaging (SENSE). The possibility of covering the whole brain in 0.5 sec on a clinical system makes this sequence a good candidate for event-related fMRI or bolus-tracking perfusion studies.

REFERENCES

1. Yang QX, Dardzinski BJ, Li S, Eslinger PJ, Smith MB. Multi-gradient echo with susceptibility inhomogeneity compensation (MGESIC): demonstration of fMRI in the olfactory cortex at 3.0 T. Magn Reson Med 1997;37:331–335.
2. Yang QX, Williams GD, Demeure RJ, Mosher TJ, Smith MB. Removal of local field gradient artifacts in T_2^*-weighted images at high fields by gradient-echo slice excitation profile imaging. Magn Reson Med 1998; 39:402–409.
3. Constable RT, Spencer DD. Composite image formation in z-shimmed functional MR imaging. Magn Reson Med 1999;42:110–117.
4. Glover GH. 3D z-shim method for reduction of susceptibility effects in BOLD fMRI. Magn Reson Med 1999;42:290–299.
5. Pruessmann KP, Weiger M, Scheidegger MB, Boesiger P. SENSE: sensitivity encoding for fast MRI. Magn Reson Med 1999;42:952–962.
6. Sodickson DK, Manning WJ. Simultaneous acquisition of spatial harmonics (SMASH): fast imaging with radiofrequency coil arrays. Magn Reson Med 1997;38:591–603.
7. Liu G, Sobering G, Duyn J, Moonen CTW. A functional MRI technique combining principles of echo-shifting with a train of observations (PRESTO). Magn Reson Med 1993;30:764–768.
8. van Gelderen P, Ramsey NF, Liu G, Duyn JH, Frank JA, Weinberger DR, Moonen CTW. Three-dimensional functional magnetic resonance imaging of human brain on a clinical 1.5-T scanner. Proc Natl Acad Sci USA 1995;92:6906–6910.
9. Waldvogel D, van Gelderen P, Muellbacher W, Ziemann U, Immisch I, Hallett M. The relative metabolic demand of inhibition and excitation. Nature 2000;406:995–998.

10. Warnking J, Dojat M, Guerin-Dugue A, Delon-Martin C, Olympieff S, Richard N, Chehikian A, Segebarth C. fMRI retinotopic mapping-step by step. Neuroimage 2002;17:1665–1683.
11. van Gelderen P, Grandin C, Petrella JR, Moonen CTW. Rapid three-dimensional MR imaging method for tracking a bolus of contrast agent through the brain. Radiology 2000;216:603–608.
12. Flacke S, Urbach H, Folkers PJ, Keller E, van den Brink JS, Traber F, Block W, Gieseke J, Schild HH. Ultra-fast three-dimensional MR perfusion imaging of the entire brain in acute stroke assessment. J Magn Reson Imag 2000;11:250–259.
13. Golay X, Pruessmann KP, Weiger M, Crelier GR, Folkers PJ, Kollias SS, Boesiger P. PRESTO-SENSE: an ultrafast whole-brain fMRI technique. Magn Reson Med 2000;43:779–786.
14. van Cuppen J, van Est A. Reducing MR imaging time by one-sided reconstruction. Magn Reson Imag 1987;5:526–527.
15. Liang Z-P, Boada FE, Constable RT, Haacke EM, Lauterbur PC, Smith MR. Constrained reconstruction methods in MR imaging. Rev Magn Reson 1992;4:67–185.
16. Stenger VA, Noll DC, Boada FE. Partial Fourier reconstruction for three-dimensional gradient echo functional MRI: comparison of phase correction methods. Magn Reson Med 1998;40:481–490.
17. Scheidegger MB, Maier SE, Boesiger P. FID-acquired-echos (FAcE): a short echo time imaging method for flow artefact suppression. Magn Reson Imag 1991;9:517–524.
18. Kellman P, Epstein FH, McVeigh ER. Adaptive sensitivity encoding incorporating temporal filtering (TSENSE). Magn Reson Med 2001;45: 846–852.
19. Hu X, Kim S-G. Reduction of signal fluctuations in functional MRI using navigator echoes. Magn Reson Med 1994;31:495–503.
20. Ramsey NF, van den Brink JS, van Muiswinkel AM, Folkers PJ, Moonen CTW, Jansma JM, Kahn RS. Phase navigator correction in 3D fMRI improves detection of brain activation: quantitative assessment with a graded motor activation procedure. Neuroimage 1998;8:240–248.
21. Weiger M, Pruessmann KP, Boesiger P. 2D SENSE for faster 3D MRI. Magn Reson Mat Phys Biol Med 2002;14:10–19.
22. Thevenaz P, Ruttimann UE, Unser M. A pyramid approach to subpixel registration based on intensity. IEEE Trans Med Imag 1998;7:27–41.
23. Glover GH, Li TQ, Ress D. Image-based method for retrospective correction of physiological motion effects in fMRI: RETROICOR. Magn Reson Med 2000;44:162–167.
24. Yang Y, Glover GH, van Gelderen P, Patel AC, Mattay VS, Frank JA, Duyn JH. A comparison of fast MR scan techniques for cerebral activation studies at 1.5 Tesla. Magn Reson Med 1998;39:61–67.
25. Bandettini PA, Jesmanowicz A, Wong EC, Hyde JS. Processing strategies for time-course data sets in functional MRI of the human brain. Magn Reson Med 1993;30:161–173.
26. de Zwart JA, van Gelderen P, Kellman P, Duyn JH. Application of sensitivity-encoded echo-planar imaging for blood oxygen level-dependent functional brain imaging. Magn Reson Med 2002;48:1011–1020.
27. Haacke EM, Hopkins A, Lai S, Buckley P, Friedman L, Meltzer H, Hedera P, Friedland R, Klein S, Thompson L, Detterman D, Tkach J, Lewin JS. 2D and 3D high resolution gradient echo functional imaging of the brain: venous contributions to signal in motor cortex studies. NMR Biomed 1994;7:54–62.
28. Lai S, Glover GH. Three-dimensional spiral fMRI technique: a comparison with 2D spiral acquisition. Magn Reson Med 1998;39:68–78.
29. Cho ZH, Ro YM. Reduction of susceptibility artifact in gradient-echo imaging. Magn Reson Med 1992;23:193–200.
30. Haacke EM, Tkach JA, Parrish TB. Reduction of T2* dephasing in gradient field-echo imaging. Radiology 1989;70:457–462.
31. Reichenbach JR, Venkatesan R, Yablonskiy DA, Thompson MR, Lai S, Haacke EM. Theory and application of static field inhomogeneity effects in gradient-echo imaging. J Magn Reson Imag 1997;7:266–279.
32. Denolin V, van Ham P, Metens T. 3D techniques in BOLD fMRI: comparison of PRESTO and standard EPI. In: Proc 8th Scientific Meeting ISMRM, Denver, 2000. p 939.